

# Atomistic simulations of stress and microstructure evolution during polycrystalline Ni film growth

Chun-Wei Pao

*Theoretical Division, Los Alamos National Laboratory, Los Alamos, New Mexico 87545, USA*

Stephen M. Foiles and Edmund B. Webb III

*Sandia National Laboratories, Albuquerque, New Mexico 87159, USA*

David J. Srolovitz

*Department of Physics, Yeshiva University, New York, New York 10033, USA*

Jerrold A. Floro

*Department of Materials Science and Engineering, University of Virginia, Charlottesville, Virginia 22904, USA*

(Received 23 May 2008; revised manuscript received 24 April 2009; published 18 June 2009)

Film stress and microstructure evolution during the growth of a Ni bicrystal film are investigated by molecular dynamics simulations. The nominal surface orientation of the growing film was (111) and the grain boundaries are  $\Sigma 79$  symmetrical tilt grain boundaries. The growth mode is layer by layer; two-dimensional (2D) islands nucleate on the surface, grow, and coalesce into complete layers. Grain-boundary migration near the free surface is observed as boundaries are dragged by step edges of growing 2D islands. Simulations show that the film stress-thickness product is compressive and oscillatory with a period that is approximately equal to one monolayer. Adatoms are observed to incorporate into grain boundaries and exert compressive strain on neighboring grains. Theoretical modeling demonstrates incorporated atoms are a primary source of the observed compressive stress during growth and gives predictions in very good agreement with simulation results. The oscillatory stress-thickness product is shown to be related to atoms diffusing into the grain boundary from the surface and out of the grain boundary onto the surface.

DOI: [10.1103/PhysRevB.79.224113](https://doi.org/10.1103/PhysRevB.79.224113)

PACS number(s): 68.60.Bs, 81.15.Aa, 61.72.Mm, 68.55.J–

## I. INTRODUCTION

Morphology evolution during Volmer-Weber (VW) growth exhibits three distinct regimes: at the early stage, isolated islands nucleate and grow. During the intermediate stage, growing islands impinge on each other and form grain boundaries (or fill channels, if islands are amorphous instead of crystalline). In the final stage of growth, a continuous polycrystalline (or amorphous) film thickens. *In situ* wafer curvature experiments<sup>1</sup> measure substrate curvature during growth and, from this, calculate the film stress-thickness product or the film stress; such experiments show that the film stress evolves in a similar manner for many different materials undergoing VW growth.<sup>2–10</sup> At the early stage (island nucleation/growth), compressive film stresses are observed. As islands impinge upon each other, film stress becomes tensile. When the film becomes continuous, the film stress can be either tensile or compressive depending on atomic mobility. Tensile stress is commonly observed when atomic mobility is low,<sup>2–4</sup> whereas it is compressive when the mobility is high.<sup>5–8</sup> During the final stage of VW growth, film stress changes are observed during growth interrupt experiments wherein deposition is temporarily stopped and then resumed. For high-mobility materials, growth interruption leads to the formation of large tensile stresses (or at least, compressive stress relaxation). When growth is resumed, the film stress thickness quickly returns to the level present before growth interrupt. For low-mobility materials, growth interrupt has less influence on film stress. In this

paper, we focus on understanding stress generation mechanisms for high-mobility materials.

There have been a number of mechanisms proposed to explain these experimental observations. The effect of surface stress on an island in mechanical equilibrium with the substrate was proposed to explain the compressive film stress generated during isolated island growth.<sup>11,12</sup> Other arguments invoke a combination of Laplace pressure and islands constrained to remain bound to the underlying substrate as a mechanism for compressive stress evolution.<sup>13</sup> The mechanism driving tensile film stress evolution during island impingement is generally well explained by the Hoffmann-Nix model<sup>14,15</sup> and models motivated by Hoffmann-Nix,<sup>16</sup> which propose that island impingement replaces high-energy surfaces with a low-energy grain boundary resulting in the formation of tensile stress. Recent atomistic simulation results of island coalescence stress suggested that the Hoffmann-Nix model overestimates the spontaneous coalescence gap and therefore significantly overestimates the island coalescence stresses.<sup>17</sup> On the other hand, mechanisms driving film stress evolution during the final stage of VW growth (when continuous polycrystalline films thicken) are not as well understood. Several mechanisms have been proposed. One model advances that as polycrystalline films thicken, grain size increases and therefore the lattice parameter of film atoms inside grains should expand (reduction in grain-boundary capillarity). However, because the film is bound to the substrate, the lattice parameter of the film cannot expand freely introducing compressive stresses.<sup>13,18</sup> This model is promis-

ing for both the initial and final stages of VW growth. However, there exists no direct evidence demonstrating that the lattice parameter of a film is locked during growth. In addition, this model cannot explain the observed tensile relaxation during growth interrupt. Another model considers the surface stress decreases due to the presence of a high density of surface defects such as surface steps, adatoms, etc.<sup>9,19,20</sup> Though this model can explain growth stress generation and tensile relaxation during interrupt, recent atomistic calculations suggest that effects of these surface defects on surface stress are too small compared with magnitudes observed in experiments.<sup>21</sup>

Chason *et al.*<sup>22</sup> proposed a model for stress evolution based on adatoms diffusing in and out of grain boundaries during growth and interrupt, respectively. In this model, the direction of adatom diffusion is determined by differences in chemical potential between the film surface and grain boundaries. During growth, an atomic flux makes the chemical potential of the growing surface higher than grain boundaries (high density of adatoms or defects), which is the driving force for surface adatoms to diffuse into grain boundaries. As adatoms diffuse into grain boundaries, they compress the grains on both sides of the boundary, yielding an overall compressive film stress. During growth interrupt, the surfaces heal, leading to a lower chemical potential on the surface than in the grain boundaries which causes atoms to diffuse back out from the grain boundaries onto the film surface, relieving the compressive film stress. This model can also explain tensile film stress during the late stage of VW growth for low-mobility materials by considering the competition between tensile stress generation (grain-boundary formation) and compressive stress generation (atomic diffusion between grain boundaries and growth surface).<sup>23</sup> However, this model depends upon grain-boundary diffusion, which, until recently,<sup>24</sup> was considered too slow compared with the time scale for stress relaxation in experiments.<sup>25</sup> Thus, another model assuming negligible grain-boundary diffusion has been proposed.<sup>26</sup> Nevertheless, mechanisms leading to compressive film stress generation during the final stage of VW growth of high-mobility materials are still unclear.

In our previous Letter,<sup>27</sup> we discussed the relation between adatoms inserting inside grain boundaries and thin-film stress. In this paper, we consider the mechanism for compressive stress generation in much more detail, in order to develop a deeper theoretical foundation. This is important, given the controversy in the literature on the origins of the development of compressive stress during film growth and should aid in devising experiments that can confirm (or contradict) theory. We also present observations of grain-boundary migration driven by the advancement of surface steps during film deposition. In the next section, we describe the simulation methods employed. This is followed by a discussion of grain-boundary migration due to film growth. Then, we present data for the evolution of the stress-thickness product during simulated deposition. To elucidate the source of compressive film stress the average displacement field of the film and atomistic configuration of grain boundary after deposition are presented. After we make the quantitative connection between excess grain-boundary den-

sity and mean stress, we discuss in detail the driving forces for adatom insertion into grain boundaries, the nature of discrepancies between experiment and theory, and stress relaxation kinetics.

## II. SIMULATION METHODS

To simulate growth of a polycrystalline film, we deposited adatoms at random locations on the surface of a Ni bicrystal film. The surface was intersected by two  $\Sigma 79[111]$  symmetric tilt grain boundaries with misorientation  $\theta=33.99^\circ$  (as shown in Fig. 1); periodic boundary conditions were applied along  $X$  and  $Y$  directions. Note that the system dimension in  $Z$  was 18 nm but only part of this is rendered in Fig. 1.<sup>28</sup> We ran molecular dynamics at constant temperature ( $T=0.5T_m$  of Ni that is,  $T=782.5$  K) prior to deposition to relax the system; all subsequent deposition simulations were run under these same conditions but the thermostat algorithm was not applied to the atom currently being deposited. The interaction between the Ni atoms was simulated using the Voter-Chen-type embedded atom method potential.<sup>29,30</sup> Three deposition simulations were performed: these are distinguished from one another by the grain size simulated,  $L$ , and the effective deposition rate (the inverse of the time between successive deposition events,  $\Delta t$ ). The first simulation with  $L=5.5$  nm and  $\Delta t=25$  ps is system A; the second simulation with  $L=11$  nm and  $\Delta t=50$  ps is system B; the third simulation with  $L=11$  nm and  $\Delta t=12$  ps is system C. Note that the first and third deposition simulations (i.e., systems A and C) had the same deposition flux. For the 5.5 nm grain-size case (system A), the total deposited film thickness  $t_f$  was three monolayers (ML), while for the 11 nm cases (systems B and C) the total deposited film thickness  $t_f$  was two monolayers. Our original Letter<sup>27</sup> only considered system B.

The stress-thickness product was obtained from simulations via a method described in Refs. 11 and 12. We calculated the difference in the average force in  $X$  across a series of imaginary cutting planes normal along  $X$  before and after deposition. That is,  $\Delta\sigma_{xx}h=(F_x-F_x^0)/L_y$ , where  $\Delta\sigma_{xx}h$  is the change in stress-thickness product compared with the initial continuous film (an absolute value of stress-thickness product cannot be given since we do not begin with a singular, pristine, clean substrate surface before deposition),  $F_x(F_x^0)$  is the force in  $X$  after (before) deposition and  $L_y$  is the simulation cell width along  $Y$ .

## III. SURFACE MORPHOLOGIES AND GRAIN-BOUNDARIES MIGRATION

Figure 1 shows surface morphology evolution of systems B and C. In Fig. 1, atoms are shaded according to their centrosymmetry parameter<sup>31</sup> and only atoms with centrosymmetry greater than 6.0 are displayed (centrosymmetry equals zero for atoms in an ideal, bulk FCC environment; larger centrosymmetry parameter values indicate more significant deviations from the ideal, bulk environment). Atoms at grain boundaries are colored dark gray while atoms on the surface are light gray. From Fig. 1 it can be observed that growth is layer by layer, which is due to significant atomic mobility on

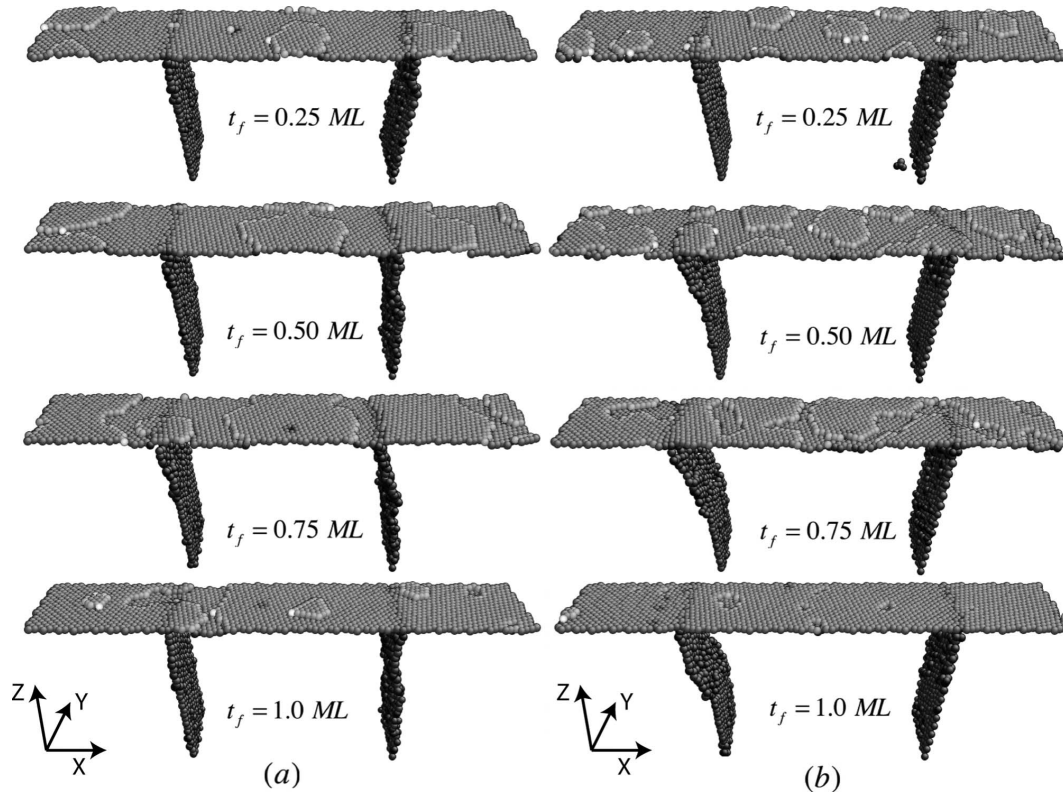


FIG. 1. Images of the atomic structure of the simulation cell during deposition simulations on  $L=11$  nm grain systems for varying coverage. Only surface atoms (colored in light gray) and grain-boundary atoms (dark gray) are presented (a) relaxation time  $\Delta t=50$  ps (system B); (b) relaxation time  $\Delta t=12$  ps (system C). Axes below show the coordinate system of the simulations.

the  $\{111\}$  surface at the high simulation temperature. By comparing Figs. 1(a) and 1(b) it can be seen that the surface for system B is smoother (i.e., smaller step density) than system C because higher deposition rate in the latter system means adatoms have less time to sample the surface before the next adatom arrives. As such, the probability for new two-dimensional (2D) islands and steps to nucleate is higher for increased deposition rate. Examination of Figs. 1(a) and 1(b) also shows that grain boundaries near the surface migrate. As 2D-surface islands grow, island step edges drag grain boundaries near the surface along with advancing step edges. This observation is similar to what was seen experimentally by Ling *et al.*<sup>32</sup> and it shows a possible mechanism for grain growth during polycrystalline film growth.

In our model, steps drag grain boundaries along with their advance because a surface 2D island with a grain boundary cutting through it has higher energy than an island with grain boundary cutting through the island edges (i.e., it is energetically favorable for islands to remain “single-crystal”). Thus, grain boundaries are attracted to step edges and repelled by step interiors; as a result, boundaries try to remain physically near island-step edges and, as islands grow, grain boundaries are dragged with advancing steps. However, there is also an energetic penalty from bending initially straight grain boundaries. This is proportional to the boundary curvature and so its magnitude, especially local to the surface, may become significant for the degree of bending observed in simulations. It should be noted that, during deposition, kinetic effects in conjunction with the penalty for boundary bending can over-

ride thermodynamic effects such that we sometimes observe islands with grain boundaries cutting through them.

#### IV. STRESS EVOLUTION

Figure 2 shows the change in stress-thickness product  $\Delta\sigma_{xx}h$  as a function of deposited film thickness  $t_f$  for systems A, B, and C. Though there are oscillations in the stress-thickness curves for all three simulations, the stress thickness

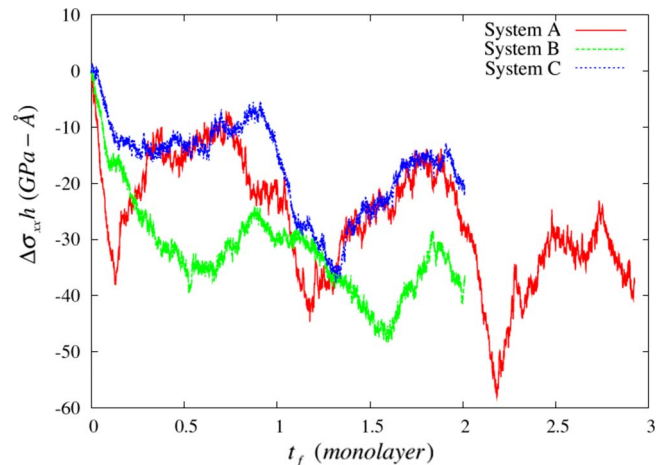


FIG. 2. (Color online) The change in film stress-thickness product  $\Delta\sigma_{xx}h$  with respect to the deposited film thickness  $t_f$ . This figure is Fig. 2 in Ref. 27.

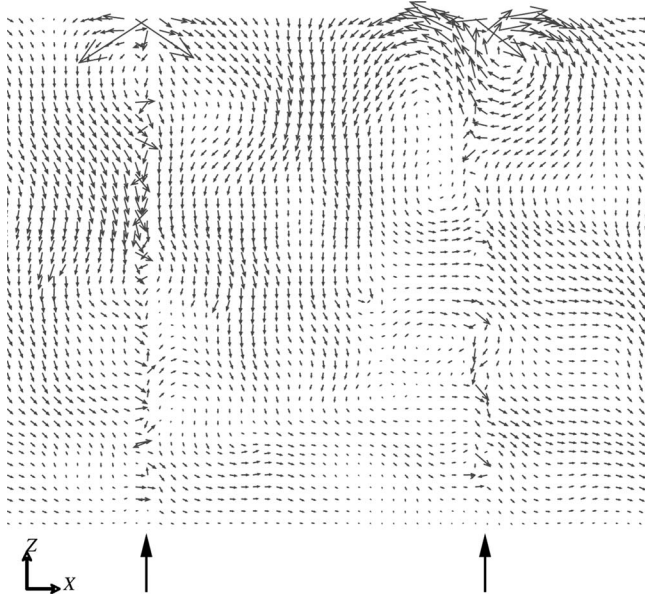


FIG. 3. The average displacement field of atoms in a  $t_f=0.09$  ML film relative to that at  $t_f=0$  ML. Each vector represents the average atomic displacement within a cell of size  $4 \times L_y \times 4 \text{ \AA}^3$  ( $L_y$  is the cell length along  $Y$ ). Two arrows, below, highlight the grain-boundaries locations.

is negative (i.e., compressive film stress); this is consistent with wafer curvature experiment results for high-mobility materials. Further examination of the stress-thickness curves shows oscillations have a periodicity roughly equal to one monolayer; as discussed further below, this is related to the layer-by-layer growth mode in our simulations. To compare the magnitude of the compressive film stress obtained in the present study with experiments, the incremental film stress (the derivative of the stress-thickness curve)  $\sigma_{xx}^{\text{inc}}$ , can be written approximately as  $\sigma_{xx}^{\text{inc}} \approx [\Delta\sigma_{xx}h(t_f=2.0 \text{ ML}) - \Delta\sigma_{xx}h(t_f=1.0 \text{ ML})]/\Delta t_f$ . Using this approximate incre-

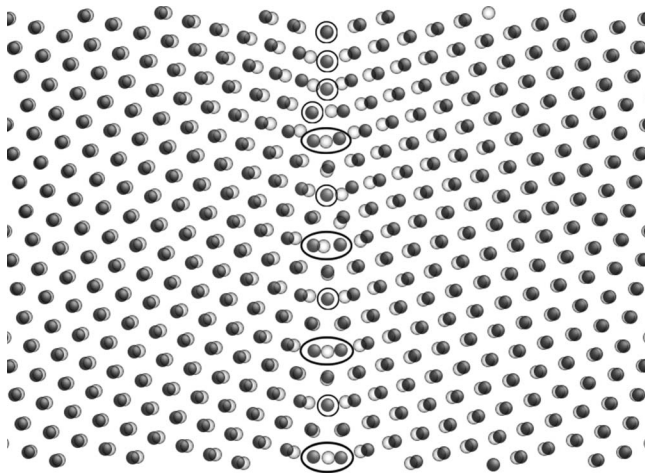


FIG. 4. A view of the atom positions (along  $Z$ ) one layer below the surface in the vicinity of the grain boundary shown on the right in Fig. 3; atoms are rendered for  $t_f=0$  ML (white) and  $t_f=0.09$  ML (gray). Regions with extra atoms are highlighted with black circles and ovals.

mental stress for all three simulations we find  $\sigma_{xx}^{\text{inc}} \approx -3.14$  GPa in system A,  $\sigma_{xx}^{\text{inc}} \approx -3.23$  GPa in system B, and  $\sigma_{xx}^{\text{inc}} \approx -3.11$  GPa in system C. Comparing systems B and C, we see that slower deposition rates yield larger compressive stresses, which is consistent with experimental observations. Incremental film stress observed in the present study ( $-3$  GPa) is much larger than observed in experiments (less than  $-1$  GPa). We attribute this to differences in surface growth morphologies between our simulations and real experiments and address this further below.

To elucidate the source of compressive film stress, the average displacement field of film atoms between  $t_f=0.09$  and  $t_f=0$  ML was calculated. Results are shown for system B in Fig. 3 wherein one can see that both grains are under compression near the surface. The grain boundary on the right of Fig. 3 exerts significant compressive strain on neighboring grains, while the grain boundary on the left exerts a relatively smaller compressive strain. Effects of strain are mainly localized to atomic layers near the free surface. The displacement field suggests the possibility that adatoms incorporating into grain boundaries produce compression observed in Figs. 2 and 3. To address this, atomistic configurations of the subsurface atomic layer of the right grain boundary shown in Figs. 1(a) and 3 are shown in Fig. 4. White atoms show the configuration at  $t_f=0$  ML while gray atoms show  $t_f=0.09$  ML. Figure 4 shows that extra atoms are inside the grain boundary (extra atoms—atoms not part of the perfect crystal—are highlighted by circles and ovals). Furthermore, the displacement of atoms outside the grain boundary clearly demonstrates both grains are subjected to compressive strain due to the incorporation of these extra atoms.

## V. GRAIN-BOUNDARY ATOM INCORPORATION

To quantitatively assess atom incorporation into grain boundaries, the number of atoms along the thickness of the film was computed by counting the number of atoms per (111) atomic layer,  $N$ , as a function of depth from the surface,  $D$ . Figures 5(a)–5(c) show results of these analyses for all three simulation conditions at different  $t_f$ ; in all figures the distribution at  $t_f=0$  ML,  $N_0(D)$ , is also plotted for comparison. Note that  $D=0$  corresponds to the free-surface position; growing surface-layer atoms are excluded from this analysis. Figures 5(a)–5(c) show that near the surface there are excess atoms compared with the perfect crystal (i.e., prior to deposition). This is further evidence of adatom incorporation into grain boundaries since we almost never observe bulk self-interstitials in our simulations. By comparing distributions between  $t_f=0.64$  and  $0.85$  ML in Figs. 5(b) and 5(c) and between  $t_f=0.14$  and  $0.72$  ML in Fig. 5(a), one can see that the number of atoms incorporated into grain boundaries decreases. That is, during deposition some atoms that have incorporated into grain boundaries escape back to the surface. By comparing these figures with Fig. 2 it can be seen that stress thickness becomes less compressive when the number of extra atoms incorporated within grain boundaries decreases. Figures 5(a)–5(c) show the penetration depth of the extra atoms is about  $10 \text{ \AA}$  for system A, while extra

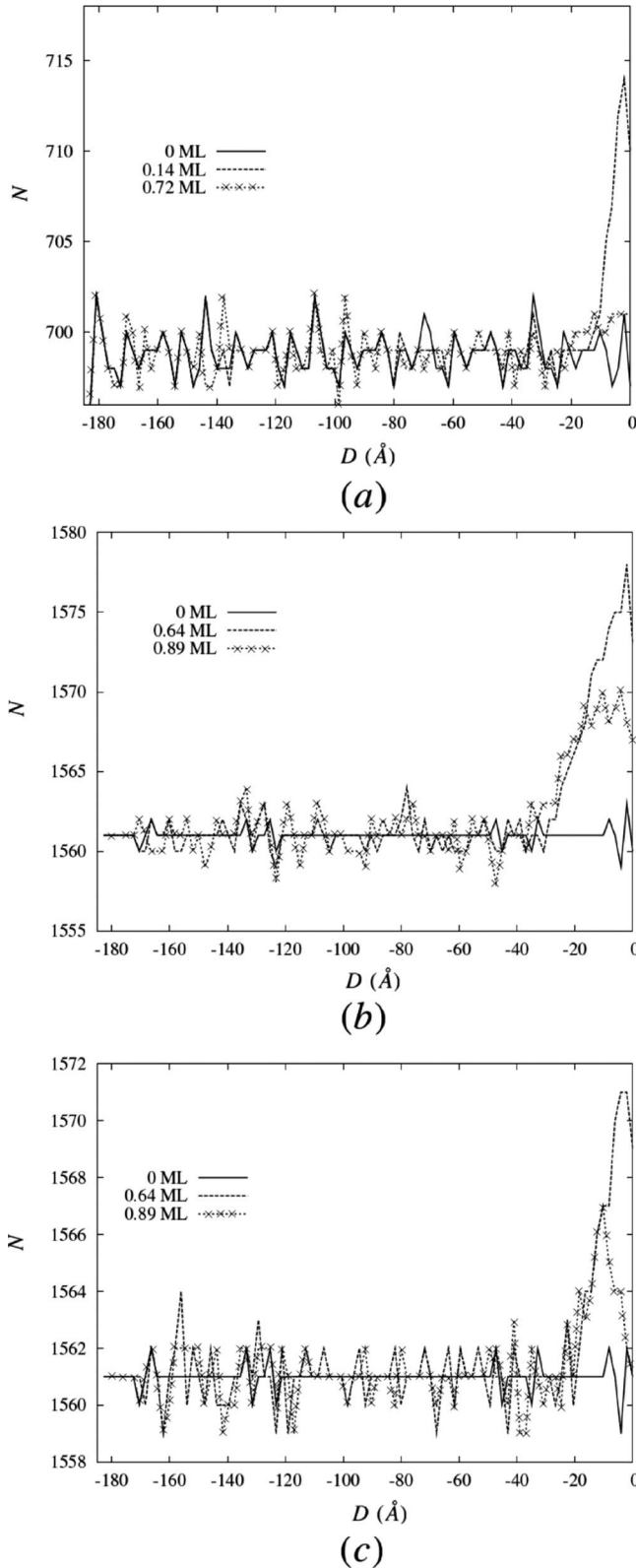


FIG. 5. Distribution of the number of atoms  $N$  along the thickness of the film for systems A, B, and C with respect to depth from the free-surface  $D$ . Note  $D=0$  refers to the free surface. (a) system A with  $t_f=0, 0.14,$  and  $0.72$  ML; (b) system B with  $t_f=0, 0.64,$  and  $0.89$  ML; (c) system C with  $t_f=0, 0.64,$  and  $0.89$  ML. Figure 5(b) is modified from Fig. 3a in Ref. 27.

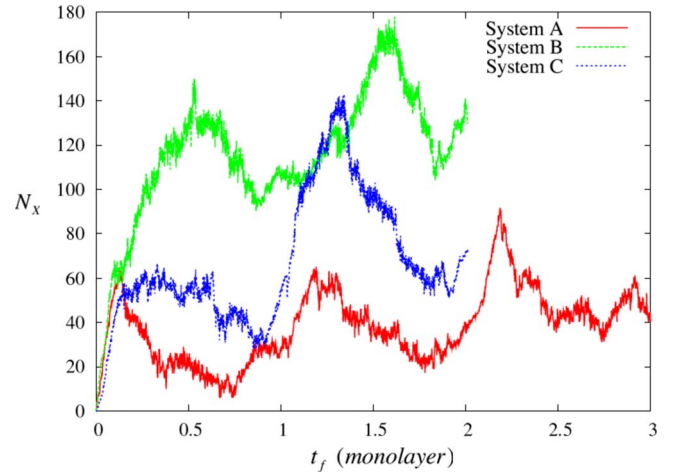


FIG. 6. (Color online) Number of extra atoms inside the film (i.e., at the grain boundaries)  $N_X$  vs deposited film thickness  $t_f$  for all three simulations. This figure is Fig. 3b in Ref. 27.

atoms penetrate  $25 \text{ \AA}$  for system B and  $20 \text{ \AA}$  for system C. It is worth noting that significant compressive stress is observed though extra atoms only penetrate into grain boundaries to a relatively small depth.

For a given  $t_f$ , we compute the total number of extra atoms incorporated into grain boundaries by integrating the difference between  $N(D)$  and  $N_0(D)$ ; that is,  $N_X = \sum_D [N(D) - N_0(D)]$ , where  $N_X$  is the total number of extra atoms inside the film. As mentioned above, bulk self-interstitials are rarely observed in our simulations so we attribute all  $N_X$  atoms to grain-boundary incorporation. Figure 6 shows  $N_X$  as a function of  $t_f$  for all three simulations. This figure shows that  $N_X$  gradually increases though oscillations are observed, emphasizing that incorporated atoms sometimes migrate back to the surface. By comparing Figs. 2 and 6 one can note an apparent inverse relation between  $\Delta\sigma_{xx}h$  and  $N_X$ . We explore this further in the following section.

## VI. RELATION BETWEEN STRESS EVOLUTION AND ATOM INCORPORATION

The simulation data above show that there is an inverse correlation between  $\Delta\sigma_{xx}h$  and  $N_X$ . The stress associated with the extra atoms inside the grain boundaries can be approximated as

$$\sigma_{xx} \approx -E \frac{a-d}{L+d} N_X \left( \frac{\pi a^2}{4} \right), \quad (1)$$

where  $E$  is the elastic (Young's) modulus,  $d$  is the "width" of the grain boundary,  $L$  is the grain size,  $a$  is the diameter of an atom, and  $L_y$  is the simulation cell size in the  $Y$  direction. Note that  $d$  is related to the free volume of a grain boundary via  $v=L_yhd$  and therefore is a characteristic of the grain-boundary type; simulations and experiments routinely show that  $d$  is a fraction of  $a$ . In Eq. (1),  $(a-d)/(L+d)$  is the strain that would result from insertion of a complete monolayer of adatoms in each grain boundary. The term inside the bracket

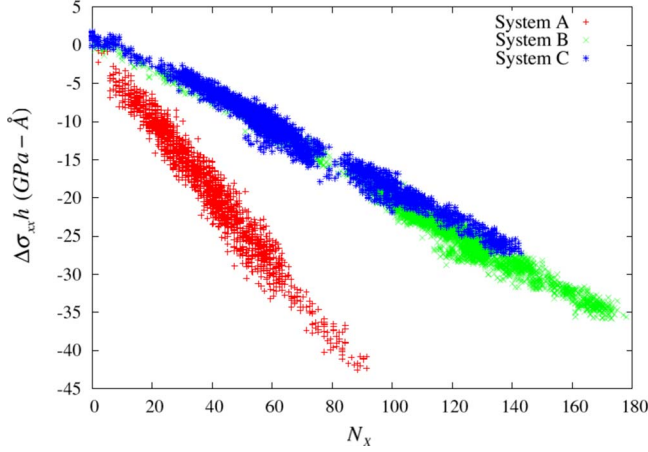


FIG. 7. (Color online)  $\Delta\sigma_{xx}h$  vs  $N_X$  for all three simulations.

on the right hand side is the fraction of grain-boundary area occupied by one incorporated atom. Thus, the part of the expression to the right of  $E$  in Eq. (1) is approximately the strain produced in the film associated with inserting a fractional monolayer of adatoms in each grain boundary. Assuming  $L \gg d$ , we can simplify this equation as

$$\sigma_{xx} \approx -E \frac{a \left(1 - \frac{d}{a}\right)}{L} N_X \left(\frac{\pi a^2}{8hL_y}\right). \quad (2)$$

Thus, we have the stress-thickness product

$$\sigma_{xx}h \approx -E \frac{\pi a^3 \left(1 - \frac{d}{a}\right)}{4L_x L_y} N_X. \quad (3)$$

Note that  $2L=L_x$ , where  $L_x$  is the simulation cell length along the  $X$  direction. In Eq. (3) the parameter  $[\pi(1-d/a)]/4$  is the same as the geometrical parameter  $\alpha$  in the grain-boundary insertion model.<sup>22</sup> Thus, we can interpret  $\alpha$  as a parameter that is inversely related to the free volume of a grain boundary. Smaller grain boundary free volume means smaller width  $d$  and therefore higher  $\alpha$ . From Eq. (3) it can be seen that the stress-thickness product is a linear function of  $N_X$  with slope  $-E\pi a^3(1-d/a)/4L_x L_y$ . In addition, for a given grain-size  $L$  the slope will be the same regardless of deposition rate. Conversely, for a given  $N_X$ , smaller grain sizes will yield larger compressive film stresses. Figure 7 shows the stress-thickness product as a function of  $N_X$  from simulations. Consistent with the prediction in Eq. (3), the stress-thickness product is a linear function of  $N_X$ . Similarly, data for systems B and C show that deposition rate does not affect the slope whereas smaller grain size in system A ( $L = 5.5$  nm) gives a larger slope than systems B and C ( $L = 11$  nm).

Equation (3) can be further simplified by introducing the quantity  $\rho_X = N_X/L_x L_y$ , which has the physical meaning of the density of extra atoms per unit film-surface area. Therefore Eq. (3) can be rewritten as

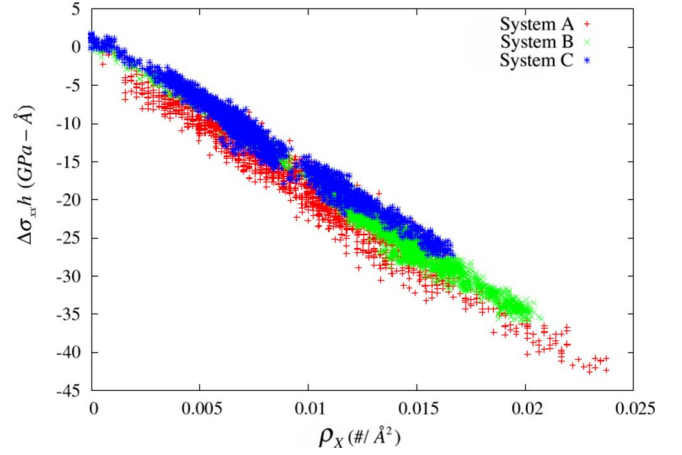


FIG. 8. (Color online)  $\Delta\sigma_{xx}h$  vs the density of extra atoms inside the film  $\rho_X$  for all three simulations. This figure is Fig. 4 in Ref. 27.

$$\sigma_{xx}h \approx -E \frac{\pi a^3}{4} \left(1 - \frac{d}{a}\right) \rho_X. \quad (4)$$

This shows that the stress-thickness product should be a linear function of  $\rho_X$ , regardless of grain size and deposition rate. To verify this prediction, we plot the stress-thickness product  $\Delta\sigma_{xx}h$  as a function of  $\rho_X$  for the three simulations in Fig. 8 from which it can be seen that data from all three simulations collapse onto a single line verifying the prediction in Eq. (4).

We further explore quantitative effects of atom incorporation by solving Eq. (4) using relevant system parameters. From separate atomistic simulations, our model gives  $a = 2.51$  Å and  $E = 191.6$  GPa. To estimate  $(1-d/a)$ , we need the grain boundary-width  $d$  obtained from the grain-boundary free volume  $v = dL_y h$ . To compute  $v$ , we compare the volume at zero pressure for a system containing grain boundaries (but no free surfaces) to the volume of the same number of atoms but in an ideal bulk face-centered cubic (FCC) crystal. In this fashion,  $d$  obtained is 0.31 Å. With these quantities, the theoretical model predicts a slope for data in Fig. 8 of  $-2099$  GPa-Å<sup>3</sup>; this compares to a best-fit slope for data in Fig. 8 of  $-1817$  GPa-Å<sup>3</sup>. The prediction of the theoretical model is 16% greater than the best fit to data; given the simplistic approximations made for the strain acting on the grains, this is very good agreement. Thus, we have found a quantitative connection between extra atoms incorporated into grain boundaries and the development of significant compressive film stress evolution.

## VII. DISCUSSION

We return to the oscillatory behavior in the number of extra atoms incorporated at grain boundaries,  $N_X$  (i.e., extra atoms entering and exiting grain boundaries). This behavior is directly related to the oscillatory feature of the stress-thickness product so it is of interest to more thoroughly understand why atoms that diffused from the surface into the grain boundary periodically escape from the grain bound-

aries and go back to the surface. We can understand this phenomenon by considering the chemical potentials of the grain boundary and the surface. More specifically, we consider the chemical potential for atoms on the edge of a 2D island on the surface  $\mu_i$ , which can be written as (assuming a circular island)

$$\mu_i = \mu_i^0 + \frac{\gamma_i \Omega}{R}, \quad (5)$$

where  $\mu_i^0$  is the chemical potential of atoms on a flat surface,  $\gamma_i$  is the surface energy of the edge of the 2D island,  $\Omega$  is the atomic volume, and  $R$  is the island radius. The chemical potential expression in Eq. (5) is for surface under thermal equilibrium. However, since the temperature of our simulation is very high, it is easy for the system to reach equilibrium configurations and therefore Eq. (5) is a reasonable approximation. From this it can be seen that the chemical potential of atoms in a 2D island decreases as the island grows. The chemical potential of extra atoms in a grain boundary can be written as

$$\mu_{gb} = \mu_{gb}^0 - \sigma_{xx} \Omega = \mu_{gb}^0 + E \frac{\pi a^3 \left(1 - \frac{d}{a}\right) \Omega}{8LL_y h} N_X, \quad (6)$$

where  $\mu_{gb}^0$  is the chemical potential of atoms inside the grain boundary without straining neighboring grains and  $\Omega$  refers to the atomic volume of the extra atom. We can see  $\mu_{gb}$  increases with  $N_X$ . Note that  $\mu_i^0 > \mu_{gb}^0$  is often satisfied because atoms at the surface have fewer neighbors than inside grain boundaries.

Consider, for example, the earliest stage of deposition when the islands on the surface are very small (initially single adatoms). In this case, the chemical potential of island atoms will be very large and likely much larger than atoms at the grain boundary, i.e.,  $\mu_i > \mu_{gb}$ . Therefore, adatoms will diffuse into grain boundaries. However, as  $N_X$  increases  $\mu_{gb}$  also increases due to increasing strain energy. As the size of the 2D islands on the surface grow,  $\mu_i$  gets smaller (in fact, if islands impinge upon one another and atoms attach to the edges of holes in the nearly continuous surface layer,  $\mu_i < \mu_i^0$  since  $R$  is effectively negative). Thus, at some point, when enough adatoms enter the boundary and/or the island grows large enough, the situation reverses and  $\mu_i < \mu_{gb}$ , such that atoms will diffuse from the grain boundary back to the surface and attach to surface islands. The chemical potential on the surface is a minimum when the surface layer is nearly complete (assuming layer-by-layer growth). This means that the number of atoms in the grain boundary and the compressive stress in the grains should be a minimum near integer values of  $t_f$ . This is consistent with the observed minima in the  $N_X$  oscillations in Fig. 6 that occurs when atomic layers are nearly full (integer values of  $t_f$ ).

The incremental film stress  $\sigma_{xx}^{\text{inc}}$  measured in the present simulations is at least three times larger than those measured in physical deposition experiments. This discrepancy may be related to the idealized surface morphologies in the simula-

tions. To demonstrate this, take the derivative of both sides of Eq. (4) with respect to film thickness. This yields an expression for the incremental film stress  $\sigma_{xx}^{\text{inc}}$

$$\sigma_{xx}^{\text{inc}} = \frac{d\sigma_{xx} h}{dt_f} = -E \frac{\pi a^3}{4} \left(1 - \frac{d}{a}\right) \frac{d\rho_X}{dt_f}. \quad (7)$$

Thus incremental film stress is directly proportional to the rate of incorporation of extra atoms into grain boundaries  $d\rho_X/dt_f$ . Any effects due to grain size and deposition rate are captured by  $d\rho_X/dt_f$ ; therefore, this expression should be suitable for any growth condition. Surface steps are a sink for surface adatoms. Thus higher surface-step density means adatoms are less likely to find grain boundaries before being “trapped” by a step. This means a lower rate of incorporation and smaller incremental film stress as was seen upon comparing systems B and C in Figs. 1 and 6. Comparison of system B and C morphologies can be extended to more realistic polycrystalline film growth. In this case, the surface has a much higher step density (e.g., a “wedding cake” morphology)<sup>33</sup> than seen in the simulations. Thus, it is much less likely that adatoms will find a grain boundary before attaching to a step under more realistic growth conditions. The resulting smaller rate of incorporation gives significantly lower incremental film stress in experiments.

In the literature associated with the development of residual stress in thin films, a distinction has been drawn between two generic types of stress evolution behavior. Low adatom mobility film growth results only in the development of tensile stress,<sup>2-4</sup> with no stress relaxation during growth interrupts. High adatom mobility film growth results in the development of compressive stress in the fully coalesced film (after the initial net tension due to coalescence),<sup>5-8</sup> with relaxation of the compression observed during interrupts. For example, Fe grown at room temperature in ultrahigh vacuum exhibits low-mobility behavior, while Fe grown at 300 °C exhibits high-mobility behavior.<sup>18</sup> Within the context of the Chason model<sup>22</sup> and our simulations, low mobility implies conditions of deposition rate and temperature where grain-boundary diffusion is suppressed and where limited surface diffusion leads to significant increases in the surface step density. Both effects reduce incorporation of excess atoms in grain boundaries, preventing the development of compressive stress under these conditions. In the simulations reported here, the enormous deposition rates used in molecular dynamics are offset by the elevated deposition temperature, so that the Ni films grow under high mobility conditions as demonstrated by the ability of the surface to remain relatively smooth after deposition.

If adatom incorporation into grain boundaries is indeed the operative mechanism during polycrystalline film growth, then it should also play a role during compressive stress relaxation during growth interrupt experiments. During steady state compressive stress evolution in VW growth, each layer of deposited material should have a steady state density of incorporated atoms  $\rho_X$ . Though local variations in  $\rho_X$  may exist across the surface (e.g., for different types of grain boundaries), the average  $\rho_X$  should directly correspond to the observed incremental compressive stress. According to the mechanism proposed by Chason *et al.*, compressive film

stress relaxation during growth interrupt is due to extra atoms at grain boundaries diffusing back to the surface and thereby relaxing compressive stress acting on neighboring grains.<sup>22</sup> A primary criticism of this mechanism is that grain-boundary diffusion is not fast enough to explain the time scale of relaxation observed in experiments. In order to explore this with atomic scale simulations, an appropriate starting state and time scale must be considered. The appropriate starting state for a growth interrupt simulation is one where grain boundaries are populated, all along the film thickness, with a steady state  $\rho_X$ , corresponding to the steady state compressive stress. This is different from current simulations where a significant percentage of the grain-boundary area is unoccupied (unstrained). Furthermore, though relaxation is observed on a time scale that is considered “fast” to experiments (seconds to minutes), it is sufficiently slow to greatly challenge time scale constraints for molecular dynamics simulations. We verified these notions by performing relaxation (or interrupt) simulations on system A for several different  $t_f$  (i.e., magnitudes of  $\rho_X$  and compressive stress) with relaxation time up to 10 ns and saw no notable change in the system. Though current resources permit us to study an order of magnitude longer simulation time, we refrain due to an improper starting state. Instead we consider Figs. 5(a)–5(c), which show extra atoms diffuse 20–30 Å into grain boundaries during simulations of order tens of ns. Also, data in Fig. 8 demonstrate that modest decreases in  $\rho_X$  produce significant reduction in compressive stress; thus, it must be acknowledged that some portion of the incorporated atoms may remain in grain boundaries after compressive relaxation is complete. Further insight can be obtained by considering recent calculations demonstrating that the formation energy for self-interstitials at metal grain boundaries is significantly reduced from bulk values such that, in many cases, it is less than the formation energy for a single atom on the surface.<sup>24,34</sup> If a source of interstitials exists (say, from surface deposition onto a growing grain boundary), then the energy calculations in Refs. 24 and 34 highlight that an equilibrium composition of “thermal interstitials” may exist in grain boundaries, after deposition is halted and any relaxation is complete. Data in Refs. 24 and 34 also illustrate how self-interstitials at grain boundaries exhibit fairly large diffusivities including complex multiple atom (i.e., collective) jump mechanisms. Thus, these calculations might provide guidance for understanding atomic migration along grain boundaries during growth interrupt. Because the grain boundary is populated with incorporated atoms prior to interrupt, collective diffusion mechanisms may be operative and provide rapid atomic depletion over long segments of the grain boundary. Depletion need not be complete, though, so

these same collective atomic transport mechanisms provide for rapid repopulation of the grain boundary (and, therefore, resumption of stress level) upon continuation of growth.

Finally, recently there was a continuum model of the stress and island shape evolution during Volmer-Weber growth processes.<sup>35</sup> Almost all parameters used in this model, including the parameters required for the cohesive law employed,<sup>36</sup> can be obtained from separate atomistic scale calculations.<sup>17,34</sup> This opens a new door of bridging atomistic scale simulations and continuum level modeling and can provide valuable insights of the nature of stress evolution during Volmer-Weber growth.

### VIII. CONCLUSION

We performed molecular dynamics simulations of the deposition of Ni atoms onto the surface of a Ni bicrystal containing a pair of  $\Sigma 79$  symmetric tilt grain boundaries. We observed grain-boundary migration near the free surface and this motion was coupled to the advance of step edges/growth of 2D-surface islands. This new mechanism for grain growth during polycrystalline film growth is supported by recent experimental observations (Ling *et al.*<sup>32</sup>). Consistent with experiments that measure *in situ* film growth stress, the stress-thickness product was compressive in all simulations. However, unlike in experiments where the stress-thickness product decreases monotonically during postcontinuous film growth, the simulation showed superimposed oscillations in the stress-thickness product with a period that was roughly equal to one monolayer. This discrepancy was shown to be associated with the near perfect layer-by-layer growth in our simulations, as compared to in polycrystalline film growth experiments, where step density is much higher. Compressive stress in the simulations was shown to be the result of the incorporation of “extra” atoms into grain boundaries during growth. Guided by simulation observations, we formulated a theoretical model in which the stress-thickness product is a linear function of  $\rho_X$ , the density of extra atoms incorporated. Our study confirms the grain-boundary insertion mechanism proposed by Chason *et al.* and provides additional insight into how the structure of a grain boundary—via its free volume—influences stress generated from atom incorporation. We also highlighted related calculations in Refs. 24 and 34 that indicate collective diffusive mechanisms may provide for rapid atomic depletion and repopulation of grain boundaries during growth interrupt and resumption. Thus, strong evidence is presented that extra atoms incorporating into grain boundaries is a primary mechanism leading to compressive film stress evolution during continuous polycrystalline film growth.

<sup>1</sup>G. G. Stoney, Proc. R. Soc. London, Ser. A **82**, 172 (1909).

<sup>2</sup>G. Thurner and R. Abermann, Thin Solid Films **192**, 277 (1990).

<sup>3</sup>H. Schneeweiss and R. Abermann, Vacuum **43**, 463 (1992).

<sup>4</sup>A. L. Shull and F. Spaepen, J. Appl. Phys. **80**, 6243 (1996).

<sup>5</sup>R. Abermann and R. Koch, Thin Solid Films **129**, 71 (1985).

<sup>6</sup>R. Abermann, Thin Solid Films **186**, 233 (1990).

<sup>7</sup>J. A. Floro, S. J. Hearne, J. A. Hunter, P. Kotula, E. Chason, S. C. Seel, and C. V. Thompson, J. Appl. Phys. **89**, 4886 (2001).

<sup>8</sup>R. Abermann, R. Kramer, and J. Maser, Thin Solid Films **52**, 215 (1978).

- <sup>9</sup>F. Spaepen, *Acta Mater.* **48**, 31 (2000).
- <sup>10</sup>J. A. Floro, P. G. Kotula, S. C. Seel, and D. J. Srolovitz, *Phys. Rev. Lett.* **91**, 096101 (2003).
- <sup>11</sup>C. W. Pao and D. J. Srolovitz, *Phys. Rev. Lett.* **96**, 186103 (2006).
- <sup>12</sup>C. W. Pao and D. J. Srolovitz, *J. Mech. Phys. Solids* **54**, 2527 (2006).
- <sup>13</sup>R. C. Cammarata, T. M. Trimble, and D. J. Srolovitz, *J. Mater. Res.* **15**, 2468 (1999).
- <sup>14</sup>R. W. Hoffman, *Thin Solid Films* **34**, 185 (1976).
- <sup>15</sup>W. D. Nix and B. M. Clemens, *J. Mater. Res.* **14**, 3467 (1999).
- <sup>16</sup>L. B. Freund and E. Chason, *J. Appl. Phys.* **89**, 4866 (2001).
- <sup>17</sup>S. C. Seel, J. J. Hoyt, E. B. Webb, and J. A. Zimmerman, *Phys. Rev. B* **73**, 245402 (2006).
- <sup>18</sup>R. Koch, D. Z. Hu, and A. K. Das, *Phys. Rev. Lett.* **94**, 146101 (2005).
- <sup>19</sup>C. Friesen and C. V. Thompson, *Phys. Rev. Lett.* **93**, 056104 (2004).
- <sup>20</sup>C. Friesen, S. C. Seel, and C. V. Thompson, *J. Appl. Phys.* **95**, 1011 (2004).
- <sup>21</sup>C. W. Pao, D. J. Srolovitz, and C. V. Thompson, *Phys. Rev. B* **74**, 155437 (2006).
- <sup>22</sup>E. Chason, B. W. Sheldon, L. B. Freund, J. A. Floro, and S. J. Hearne, *Phys. Rev. Lett.* **88**, 156103 (2002).
- <sup>23</sup>A. Bhandari, B. W. Sheldon, and S. J. Hearne, *J. Appl. Phys.* **101**, 033528 (2007).
- <sup>24</sup>A. Suzuki and Y. Mishin, *Interface Sci.* **11**, 131 (2003).
- <sup>25</sup>P. R. Guduru, E. Chason, and L. B. Freund, *J. Mech. Phys. Solids* **51**, 2127 (2003).
- <sup>26</sup>B. W. Sheldon, A. Ditkowski, R. Beresford, E. Chason, and J. Rankin, *J. Appl. Phys.* **94**, 948 (2003).
- <sup>27</sup>C. W. Pao, S. M. Foiles, E. B. Webb III, D. J. Srolovitz, and J. A. Floro, *Phys. Rev. Lett.* **99**, 036102 (2007).
- <sup>28</sup>The grain-boundary equilibration process is a complex application of Monte Carlo, molecular dynamics, and energy minimization calculations. Interested readers should direct related questions to: foiles@sandia.gov.
- <sup>29</sup>M. S. Daw, S. M. Foiles, and M. I. Baskes, *Mater. Sci. Rep.* **9**, 251 (1993).
- <sup>30</sup>S. M. Foiles and J. J. Hoyt, *Acta Mater.* **54**, 3351 (2006).
- <sup>31</sup>C. L. Kelchner, S. J. Plimpton, and J. C. Hamilton, *Phys. Rev. B* **58**, 11085 (1998).
- <sup>32</sup>W. L. Ling, N. C. Bartelt, K. F. McCarty, and C. B. Carter, *Phys. Rev. Lett.* **95**, 166105 (2005).
- <sup>33</sup>M. J. Rost, D. A. Quist, and J. W. M. Frenken, *Phys. Rev. Lett.* **91**, 026101 (2003).
- <sup>34</sup>M. R. Sorensen, Y. Mishin, and A. F. Voter, *Phys. Rev. B* **62**, 3658 (2000).
- <sup>35</sup>J. S. Tello and A. F. Bower, *J. Mech. Phys. Solids* **56**, 2727 (2008).
- <sup>36</sup>X. P. Xu and A. Needleman, *J. Mech. Phys. Solids* **42**, 1397 (1994).